

Entrainment and chaos in the pulse-driven Hodgkin-Huxley oscillator

Kevin K. Lin*

Courant Institute of Mathematical Sciences
New York University

May 9, 2005

Abstract

The original Hodgkin-Huxley model describes action potential generation in the squid giant axon and is a paradigm for conductance-based, excitable biological systems. Motivated by the recent theoretical work of Qiudong Wang and Lai-Sang Young, this paper examines the response of the Hodgkin-Huxley equations to low-frequency periodic pulsatile forcing. It is shown that

1. The pulse-driven Hodgkin-Huxley system exhibits a surprisingly wide range of qualitatively distinct behaviors, including stable entrainment (phase locking) to the input pulse train, transient chaos followed by entrainment, and fully chaotic behavior.
2. The pulse-driven Hodgkin-Huxley system prefers entrainment over chaos: most combinations of drive frequency and amplitude lead to entrainment instead of chaos.
3. These phenomena can be understood in terms of a general theory of kicked oscillators developed by Wang and Young, together with specific geometric structures in the Hodgkin-Huxley phase space.

The concept of phase resetting curves, first introduced by Winfree, plays an important role in this context. This paper discusses a simplified version of the Ermentrout-Kopell adjoint method for computing phase resetting curves; it may be easier to implement in higher-dimensional settings.

1 Introduction

The Hodgkin-Huxley equations were originally derived to describe the generation of action potentials in the squid giant axon [13]. Since Hodgkin and Huxley's pioneering work, this system of nonlinear differential equations has become a paradigm for quantitative models of conductance-based, excitable cells, and their ideas and methodology have led to models of systems like striated and cardiac muscle fibers [5]. As dynamical systems, the Hodgkin-Huxley and related equations have received much attention in the mathematical and physical literature because of the variety of biological systems they describe and the rich array of phenomena observable in these models. These phenomena include the existence of multiple time

*Address: 251 Mercer Street, New York, NY 10012, USA

E-mail: klin@cims.nyu.edu

URL: <http://www.cims.nyu.edu/~klin>

scales [5], persistent chaotic behavior under sinusoidal forcing [1, 10], coherence resonance [18], some of the clearest examples of bifurcations in biological systems [20], and the existence of horseshoes and transient chaotic behavior in the unforced Hodgkin-Huxley equations [12]. Of particular relevance here is the work of Winfree and Best on the phase resetting response of the Hodgkin-Huxley model [29, 3].¹

Motivated by the recent work of Qiudong Wang and Lai-Sang Young, this paper examines the response of the Hodgkin-Huxley equations to low-frequency, periodic, pulsatile forcing. It is shown that

1. The pulse-driven Hodgkin-Huxley system exhibits a wide range of qualitatively distinct behaviors. In particular, one can find combinations of kick amplitude and kick period to realize *any* of the following response types:
 - (a) **Entrainment:** The system entrains to the periodic impulse train, *i.e.* the system is stably periodic and its period is a rational multiple of T .
 - (b) **Transient chaos:** The system experiences a transient period of exponential instability before entraining to the input. This transient chaos is caused by a horseshoe [11].
 - (c) **Chaos:** The system becomes fully chaotic, *i.e.* it has a positive Lyapunov exponent, is exponentially mixing, and possesses a unique SRB measure [30].

These phenomena are prevalent in the sense that the corresponding subsets of (T, A) -space occupy positive area. These subsets of (T, A) -space are also roughly periodic in T . (See Figures 1 and 2.)

The possibilities enumerated above are not necessarily mutually exclusive, nor is the list necessarily complete. However, available numerical results give no indication that “mixed” responses occur in the pulse-driven Hodgkin-Huxley system, and response types other than those listed above have not been observed.

2. The pulse-driven Hodgkin-Huxley system prefers entrainment over chaos: most (though not all) combinations of T and A lead to entrainment instead of chaos.
3. These phenomena can be understood in terms of the work of Qiudong Wang and Lai-Sang Young [25, 26, 27, 28] together with geometric features specific to the Hodgkin-Huxley phase space.

Throughout, a simplified version of the Ermentrout-Kopell adjoint method [9, 4] is employed to compute phase resetting curves. This version avoids the numerical solution of boundary value problems and may be easier to implement in higher-dimensional settings.

The mathematical theory of periodically-forced oscillators has a long history. First hints that such oscillators can exhibit complex dynamics appeared in the experimental work of van der Pol and van der Mark on certain nonlinear electrical circuits [24]. Cartwright and Littlewood later proved that the van der Pol equation possesses periodic orbits with different periods in some parameter regimes, hinting at attracting sets more complex than fixed points or invariant curves. Levinson obtained detailed information for a simplified model [16]. His work, in turn, inspired Smale to introduce the general idea of a horseshoe [21], which Levi used to explain some observed phenomena in a version of the van der Pol equation [15]. The phenomena described in this paper were first discovered, in the context of a simple mechanical oscillator, by Zaslavsky [31].

¹ The work of Takabe, Aihara, and Matsumoto [22] appears to overlap with this work, possibly even substantially. But, I was unable to locate anything beyond an abstract.

In a series of recent papers, Wang and Young generalize the Benedicks-Carleson theory of the Hénon map [2] to a class of strange attractors with “toroidal” geometries [25, 28] and use this theory to obtain general results for periodically-kicked oscillators [26, 27]. The basic strategy in their analysis is to reduce the dynamics of the kicked oscillator to that of a 1-dimensional circle map. Their result is perturbative and qualitative in nature and imposes restrictions on the types of kicks which are allowed. It is difficult to check these conditions for the present model. Thus the present study relies heavily on the results of numerical simulations.

There is much prior work on the pulse-driven Hodgkin-Huxley and related systems. In particular, chaotic behavior has long been observed in numerical studies of neuronal models: in the Hodgkin-Huxley system driven by a sinusoidal current [1, 10] and in the FitzHugh-Nagumo system driven by periodic pulse trains [6].² The pulse-driven Hodgkin-Huxley system has also been studied extensively by Best [3] and Winfree [29], with a focus on “phase singularities” and the transition from “Type-1” (degree 1) to “Type-0” (degree 0) phase resetting curves. The primary contribution of the present paper is a systematic exploration of the response of the Hodgkin-Huxley system to periodic pulsatile forcing and more mathematically satisfying (albeit not yet complete) explanations of some observed phenomena.

The rest of this paper is organized as follows: Section 2 briefly reviews the Hodgkin-Huxley equations and its properties. Section 3 summarizes the ideas of Winfree concerning driven oscillators and provides a heuristic introduction to Wang-Young theory. In §4, the main numerical results are stated and explained in terms of the geometry of the Hodgkin-Huxley flow and mechanisms discovered by Wang and Young. The response of the Hodgkin-Huxley neural model to finite-duration pulses is briefly discussed in §4.5.

2 Brief review of the Hodgkin-Huxley model

This section summarizes some well-known properties of the Hodgkin-Huxley equations in the absence of external forcing.

The Hodgkin-Huxley equations model the dynamics of action-potential generation in axons with two types of gated ion channels in the cell membrane. One type of channel is specific to potassium ions, the other to sodium ions. The model keeps track of the membrane voltage v , the activity n of the potassium channels, and the activity m and inactivity h of the sodium channels. The equations are [13]

$$\begin{aligned}\dot{v} &= C^{-1} [I - \bar{g}_K n^4 (v - v_K) - \bar{g}_{Na} m^3 h (v - v_{Na}) - \bar{g}_{leak} (v - v_{leak})] \\ \dot{m} &= \alpha_m(v)(1 - m) - \beta_m(v)m \\ \dot{n} &= \alpha_n(v)(1 - n) - \beta_n(v)n \\ \dot{h} &= \alpha_h(v)(1 - h) - \beta_h(v)h\end{aligned}\tag{1}$$

where

$$\begin{aligned}\alpha_m(v) &= \Psi\left(\frac{v+25}{10}\right), & \beta_m(v) &= 4 \exp(v/18), \\ \alpha_n(v) &= 0.1 \Psi\left(\frac{v+10}{10}\right), & \beta_n(v) &= 0.125 \exp(v/80), \\ \alpha_h(v) &= 0.07 \exp(v/20), & \beta_h(v) &= \frac{1}{1 + \exp(\frac{v+30}{10})}, \\ \Psi(v) &= \frac{v}{\exp(v)-1}.\end{aligned}\tag{2}$$

The \dot{v} equation is just Kirchoff’s current law; $-I$ is the current flowing from outside the membrane into the neuron. Thus, action potentials are *downward* voltage spikes and a positive I corresponds to an *outflow* of

²Also in a version of the pulse-driven Hodgkin-Huxley system [22], but see Footnote 1.

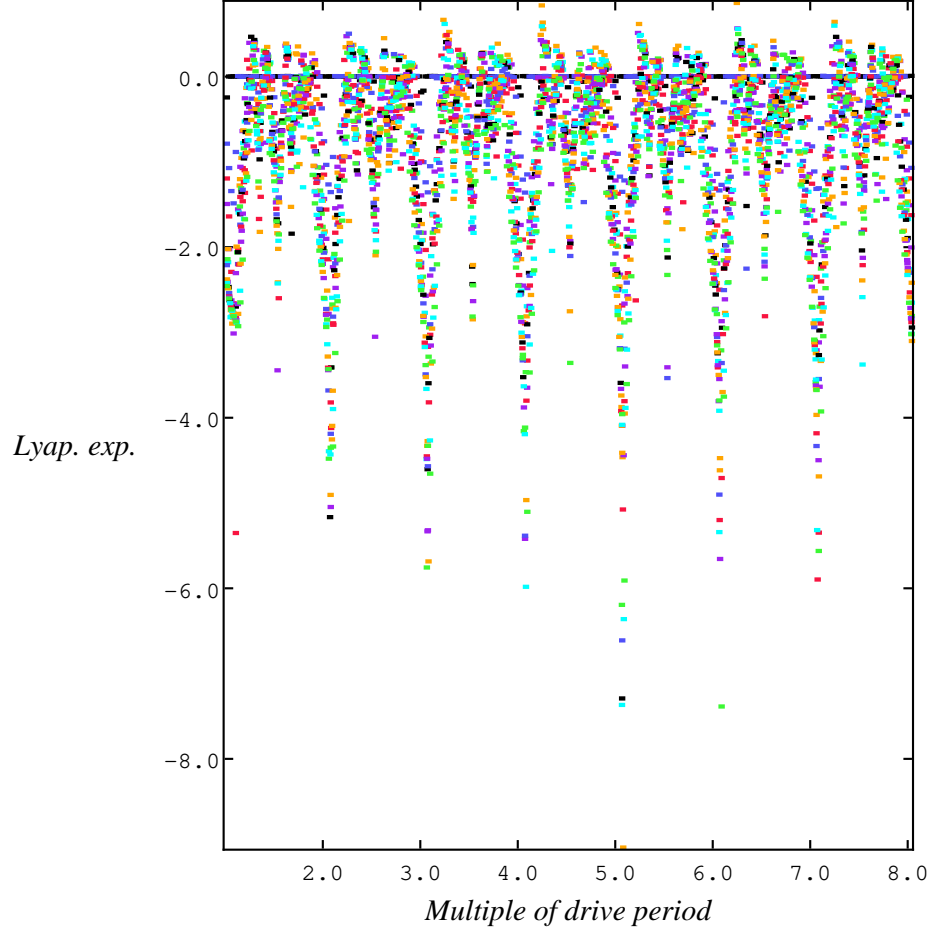


Figure 1: Asymptotic properties of the pulse-driven flow are described by the dynamics of the time- T map F_T (see §3): entrainment corresponds to F_T possessing a stable fixed point or stable periodic orbit, *i.e.* its largest Lyapunov exponent is negative, and chaos corresponds to F_T possessing a positive Lyapunov exponent. This figure shows the largest Lyapunov exponent of F_T as a function of drive period T , with T ranging from $T_\gamma \approx 13$ to $8 \cdot T_\gamma \approx 101$. Different colors correspond to different drive amplitudes A , ranging from $A = 1$ to $A = 40$. Lyapunov exponents are estimated by iterating F_T for 1000 steps and tracking the rate of growth of a tangent vector. Note that the largest Lyapunov exponent is roughly periodic in T .

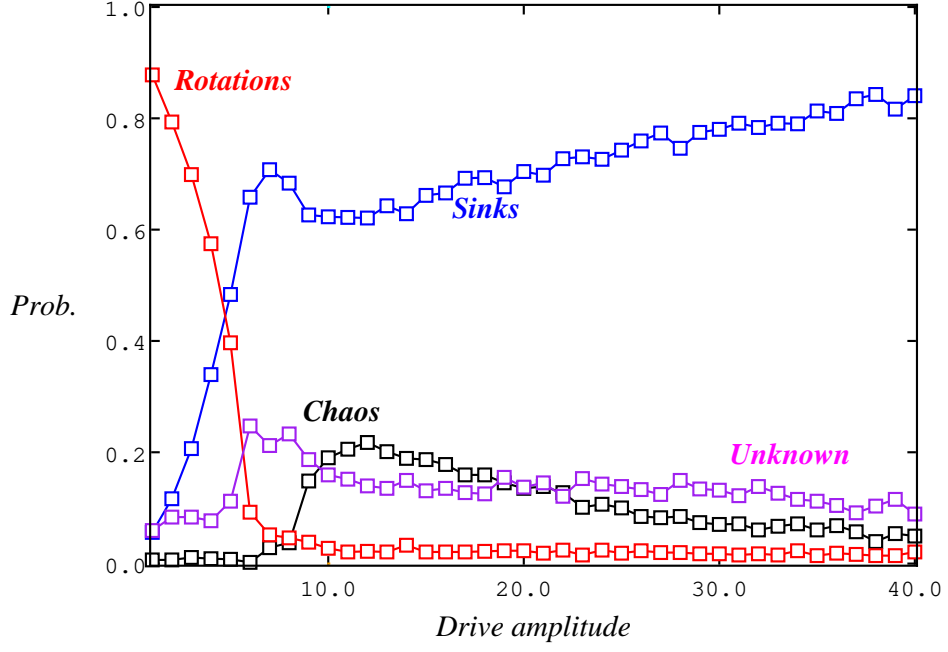


Figure 2: Drive amplitude A versus the probability of different types of asymptotic behavior of the time- T map F_T (see §3), estimated using the data shown in Figure 1. For each value of A , the fraction of T 's in the interval $[T_\gamma, 8T_\gamma]$ for which $\lambda_{\max}(F_T) > 0$, etc., is computed by sampling from a uniform grid. It is natural to equate these fractions with probabilities because the Lyapunov exponents are roughly periodic functions of T , and become more so as $T \rightarrow \infty$ (see Figure 1 and §3). *Empirical definitions:* Let $\hat{\lambda}$ denote the estimated Lyapunov exponent and ϵ the estimated standard error. Then “chaos” is defined as $\hat{\lambda} > 3\epsilon$, “entrainment” $\hat{\lambda} < -3\epsilon$, and “rotation” $|\hat{\lambda}| < \epsilon/3$.

positively-charged ions. The voltage convention here is that of [13] and opposite contemporary usage in neuroscience: the membrane voltage v is defined by

$$v = \text{voltage outside} - \text{voltage inside.}$$

Physically, the most natural form of external stimuli to neurons are perturbations of the membrane voltage. Such perturbations may be caused, for instance, by the flow of an ionic current across the membrane. Furthermore, because nerve cells transmit signals through temporally localized pulses, it is natural to model stimuli as impulses. The simplest model of a repetitive, pulsatile stimulus to a neuron is a periodic impulse train. This suggests that we replace the \dot{v} equation above by

$$\begin{aligned} \dot{v} = & C^{-1} \left[I - \bar{g}_K n^4 (v - v_K) - \bar{g}_{Na} m^3 h (v - v_{Na}) - \bar{g}_{leak} (v - v_{leak}) \right] \\ & + A \sum_{k \in \mathbb{Z}} \delta(t - kT). \end{aligned} \quad (3)$$

This defines the pulse-driven Hodgkin-Huxley system. (Section 4.5 considers finite-duration pulses, in which δ -impulses are replaced by square pulses of duration t_0 and height $1/t_0$.)

Throughout this paper, the following parameters are assumed:

$$\begin{aligned} v_{Na} &= -115 \text{ mV}, & \bar{g}_{Na} &= 120 \text{ m}\Omega^{-1}/\text{cm}^2, \\ v_K &= +12 \text{ mV}, & \bar{g}_K &= 36 \text{ m}\Omega^{-1}/\text{cm}^2, \\ v_{leak} &= -10.613 \text{ mV}, & \bar{g}_{leak} &= 0.3 \text{ m}\Omega^{-1}/\text{cm}^2, \\ C &= 1 \text{ }\mu\text{F}/\text{cm}^2. \end{aligned} \quad (4)$$

Time is measured in milliseconds and current density in $\mu\text{A}/\text{cm}^2$. For this paper, the injected current is always to $I = I_- = -14.2211827403$. This somewhat arbitrary choice corresponds to a steady outflow of positive ions and ensures that the unique fixed point (the “rest state”) is unstable. In this parameter range, there exists a stable limit cycle γ (see Figure 3). Except for I , the parameter values above come from the original paper of Hodgkin and Huxley.³ A more interesting dynamical regime may be the one considered by Guckenheimer and Oliva [12], $I = I_{co} = -7.8575590311175025$, in which a stable rest state coexists with a limit cycle and unstable cycles; see Figure 3. However, the dynamics for $I = I_-$ is easier to analyze and understand because the limit cycle γ does not coexist with a stable rest state, as it does for $I = I_{co}$.

The limit cycle describes a neuron which fires spontaneously in a repetitive manner. The Jacobian of the Hodgkin-Huxley vector field at the unstable fixed point has two real, stable eigenvalues -4.97815 , -0.146991 , and a complex conjugate pair of unstable eigenvalues $0.0763367 \pm 0.61866i$. The fixed point thus has 2-dimensional stable and unstable manifolds. The Lyapunov exponents of γ are 0 , $-0.20\dots$, $-2.0\dots$, and $-8.3\dots$. Its period is $T_\gamma \approx 12.944$.

3 Mathematical background

This section provides a brief, heuristic summary of the ideas of Winfree on phase resetting and the results of Wang and Young on kicked oscillators.

³Their value of v_{leak} does not guarantee $v = 0$ at rest state. The correct value for that is $-10.599\dots$. This is of little importance in this study, since varying the injected current I (as is done in this paper) is the same as varying v_{leak} .

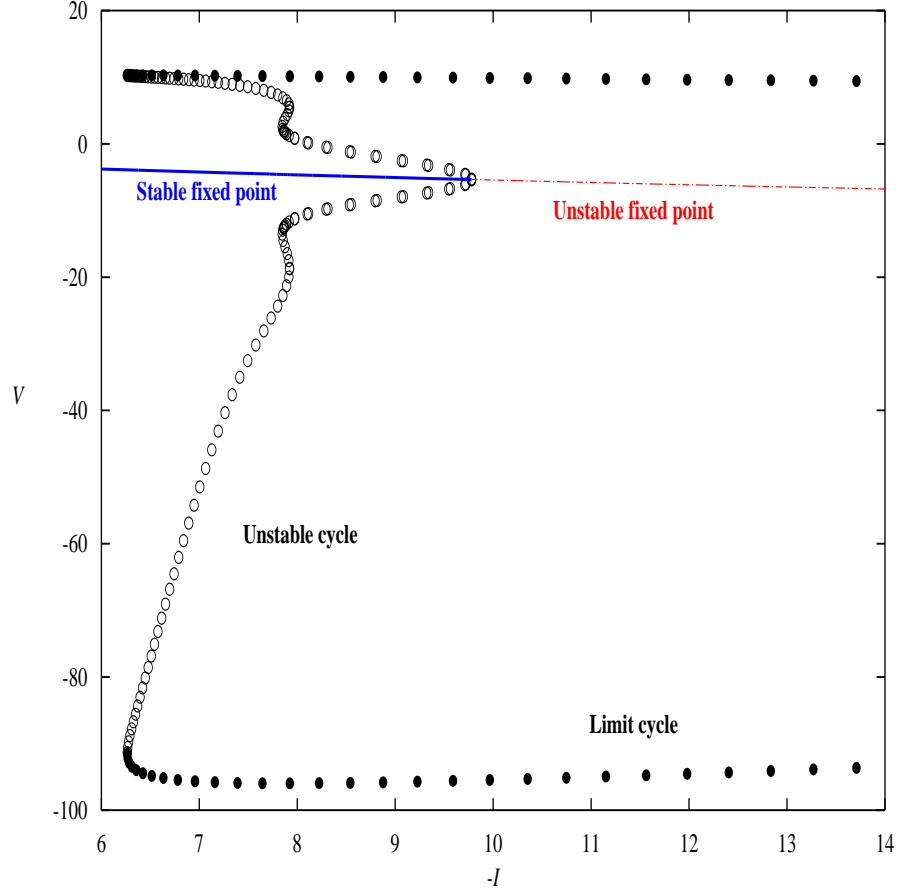


Figure 3: The bifurcation diagram for the Hodgkin-Huxley equations as the injected current $-I$ is varied. The line in the middle marks the v coordinate of the rest state. The solid blue part is stable while the dashed red part is unstable. Solid black dots near the top and the bottom of the figure are the maximum and minimum v values of limit cycles. Empty black circles are the maximum and minimum v values of unstable cycles. The fixed point undergoes a subcritical Hopf bifurcation as $-I$ increases. This diagram is computed using XPPAUT [8].

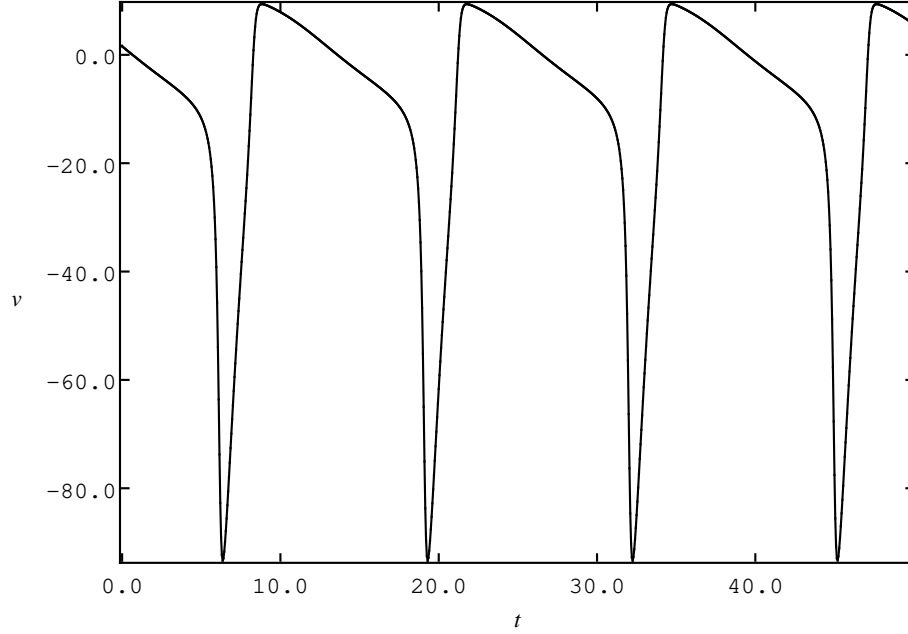


Figure 4: The time course for the Hodgkin-Huxley equations at the parameter values (4). The rapid “spike” followed by a long “refractory” period is typical of the Hodgkin-Huxley equations.

3.1 Kicked oscillators

First, some useful definitions (not all of these are in general use): a *nonlinear oscillator* is a flow Φ_t with a hyperbolic limit cycle γ of period T_γ and basin of attraction $\text{Basin}(\gamma)$. It is frequently convenient to abuse the notation γ to refer to both the periodic trajectory $\gamma : \mathbb{R} \rightarrow \mathbb{R}^n$ and to the invariant point set defined by γ . The Hodgkin-Huxley system with the value of I described in the previous section is such a nonlinear oscillator. A *kicked oscillator* is a nonlinear oscillator which periodically undergoes a discontinuous, instantaneous change of state (kicks). A periodic kick of period T can be modelled as additive forcing terms of the form $J(x) \sum_{k \in \mathbb{Z}} \delta(t - kT)$. A kicked oscillator is said to be *entrained* or *phase-locked* to its input if it is stably periodic and the period is a rational multiple of the drive period T .

It is easier to consider the dynamics of a kicked oscillator in integral multiples of the kick period T : let $K : \mathbb{R}^n \rightarrow \mathbb{R}^n$ represent the action of the kick, so that if the state of the system is x before the kick occurs, then $K(x)$ is the state after the kick. Then the map $F_T = \Phi_T \circ K$ is the time- T map of the kicked oscillator. Entrainment of the pulse-driven flow corresponds to F_T possessing a stable fixed point or stable periodic orbit, *i.e.* its largest Lyapunov exponent is negative, and chaos corresponds to F_T possessing a positive Lyapunov exponent.

The source of dynamical complexity in kicked oscillators can be illustrated by the following simple example (unrelated to the Hodgkin-Huxley equations). Consider the following equations (in polar coordi-

nates):

$$\begin{aligned}\dot{r} &= (\mu - \alpha r^2)r + Ar\phi(\theta) \sum_{n \in \mathbb{Z}} \delta(t - nT) \\ \dot{\theta} &= \omega + \beta r^2,\end{aligned}\tag{5}$$

where $\mu > 0$, ω , β are nonzero constants and ϕ is a smooth, positive, 2π -periodic function with $\min \phi < 1 < \max \phi$. When $A = 0$, this system has a limit cycle in the form of an invariant circle and an unstable fixed point at the origin. Because $\beta \neq 0$, the flow exhibits *shear*: the angular velocity $\dot{\theta}$ at a point (r, θ) depends on r , and increase monotonically with r if $\beta > 0$. When $A \neq 0$, the system is kicked periodically, and the shear and dissipation together translate the kicks into a repeated stretching and folding of the phase space around the limit cycle (see Figure 5). This, heuristically, is the source of complex dynamical behavior in the system.

Because of the inherent dissipation in the system toward the limit cycle γ , the dynamics in the basin of γ is dominated by the periodic motion along γ . This observation leads to a natural strategy for constructing a 1-dimensional system whose dynamics mimics that of the full system, by recasting the dynamics in terms of the *phase* of the oscillator. Recall that the phase $\theta : \gamma \rightarrow [0, T_\gamma)$ can be defined by first fixing a reference point $x_0 \in \gamma$ and setting the phase θ of $x \in \gamma$ to be the value of $\theta \in [0, T_\gamma)$ for which $\Phi_\theta(x_0) = x$. In the phase variable θ the unforced dynamics is trivial:

$$\frac{d}{dt}(\theta(\gamma(t))) = 1.\tag{6}$$

The phase function θ can be extended from γ to every point in its basin of attraction by projecting along strong-stable manifolds, *i.e.* if y is a point in the basin of γ then $\theta(y)$ is defined to be $\theta(x)$, where x is the unique point such that $y \in W_{ss}(x)$. This definition of phase preserves Equation (6), with γ replaced by any solution x with $x(0) \in \text{Basin}(\gamma)$.

Now consider the limit

$$\bar{F}_T = \lim_{n \rightarrow +\infty} F_{T+nT_\gamma}.\tag{7}$$

The map \bar{F}_T is well-defined on the basin of γ and retracts the basin onto γ . The map \bar{F}_T also satisfies

$$\bar{F}_T = \pi_{ss} \circ \Phi_T \circ K = \Phi_T \circ \pi_{ss} \circ K,\tag{8}$$

where $\pi_{ss}(x) = y$ if and only if $x \in W_{ss}(y)$. Since \bar{F}_T maps γ onto itself, it induces a family of maps $f_T : S^1 \rightarrow S^1$ satisfying

$$\gamma \circ f_T = \pi_{ss} \circ F_T \circ \gamma.\tag{9}$$

Clearly, $f_{T+\delta} = f_T + \delta \pmod{T_\gamma}$ and $f_{T+T_\gamma} = f_T$. Wang and Young called f_T the *singular limit* of F_T ; in Winfree's terminology, the maps f_T are *phase resetting curves*. The circle map f_T captures the dynamics of the full time- T map $F_T : \mathbb{R}^4 \rightarrow \mathbb{R}^4$ in the phase variable θ : if $\theta \in [0, T_\gamma)$ is a given phase value and $x \in \gamma$ is the corresponding point, then the phase of $\Phi_T(K(x))$ is precisely $f_T(\theta)$. The correspondence between f_T -orbits and F_T -orbits is only approximate, however, because the phase of a point x , when $x \in \text{Basin}(\gamma)$ but $x \notin \gamma$, does not fully determine the phase of $F_T(x)$; this approximation becomes exact only in the limit $T \rightarrow \infty$. By construction, the family $\{f_T\}$ is periodic in T : $f_{T+T_\gamma} = f_T$.

3.2 Wang-Young theory

For the simple example (5) above, Wang and Young proved the following: if the kick term in (5) does not send points on the limit cycle too close to the origin, then the following hold:

1. If A is sufficiently small, then F_T possesses an invariant circle $\tilde{\gamma}$ near γ for all T . The action of F_T on $\tilde{\gamma}$ is that of a circle diffeomorphism, so the standard scenarios apply:
 - (a) **Rotation-like behavior:** If F_T and all its iterates have no fixed points on $\tilde{\gamma}$, then the restriction of F_T to $\tilde{\gamma}$ is conjugate to a rigid rotation on the circle [14].
 - (b) **Entrainment (“gradient-like” behavior):** If F_T has stable fixed points or stable periodic orbits, then these invariant sets determine the asymptotic behavior of typical orbits. A stable fixed point or periodic orbit is called a *sink*, and an unstable fixed point or periodic orbit is called a *source*. An F_T -orbit falling into a sink corresponds to entrainment of the kicked oscillator to its input.
2. For larger values of A , the invariant curve is replaced by a more complicated invariant set.
 - (a) **Entrainment:** There exist T such that F_T is gradient-like, as described above.
 - (b) **Transient chaos:** There exist T for which the kicked oscillator experiences transient periods of exponential instability before entraining to the input. Mathematically, F_T possesses a horseshoe, an invariant Cantor set on which F_T is uniformly hyperbolic [11]. Because of the invariance of the horseshoe, trajectories passing near it are likely to return again, and its hyperbolicity causes nearby trajectories to separate exponentially in time.
 - (c) **Chaos:** There exist T for which the system is fully chaotic, *i.e.* F_T has a positive Lyapunov exponent, exhibits exponential decay of correlations, and possesses a unique SRB measure [30].

Furthermore, for each scenario above, the subset of (T, A) -space which realizes the scenario has positive Lebesgue measure and is roughly periodic in T .

The Wang-Young analysis (see [26, 27]) infers information about F_T from the circle map f_T . The proof of Scenario 2c, in particular, requires that $T \gg 1$ so that f_T very closely mimics F_T , although intuitively all these phenomena should be quite robust. Numerical results support this, showing that for the Hodgkin-Huxley system, the predicted phenomena are observable even when $T \approx T_\gamma$. The periodicity of f_T in T implies that the subsets of (T, A) -space corresponding to the scenarios stated above are roughly periodic in T , with period T_γ .

In order to guarantee the appearance of these phenomena, the theory places some restrictions on the types of kicks one uses. The first restriction is that the kick does not send the limit cycle outside the basin of γ . This ensures that f_T is well-defined and smooth. The second restriction is that there is sufficient shear in the flow to fold the phase space (see Figure 5), and that the kick is “radial” enough to take advantage of the shear. See [26] and [27] for details.

In addition to proving the assertions stated above, Wang and Young showed that in the case of a limit cycle emerging from a supercritical Hopf bifurcation [11], if the “twist factor” (a quantity computable through the Hopf normal form [11]) is sufficiently large, then there exist drive periods T which will induce chaotic response from the oscillator. This criterion for chaos has been applied to the Chua circuit [17] but does not apply to the Hodgkin-Huxley equations because the Hopf bifurcation which occurs here is subcritical, not supercritical. See [11] for a thorough discussion of the relevant bifurcation theory.

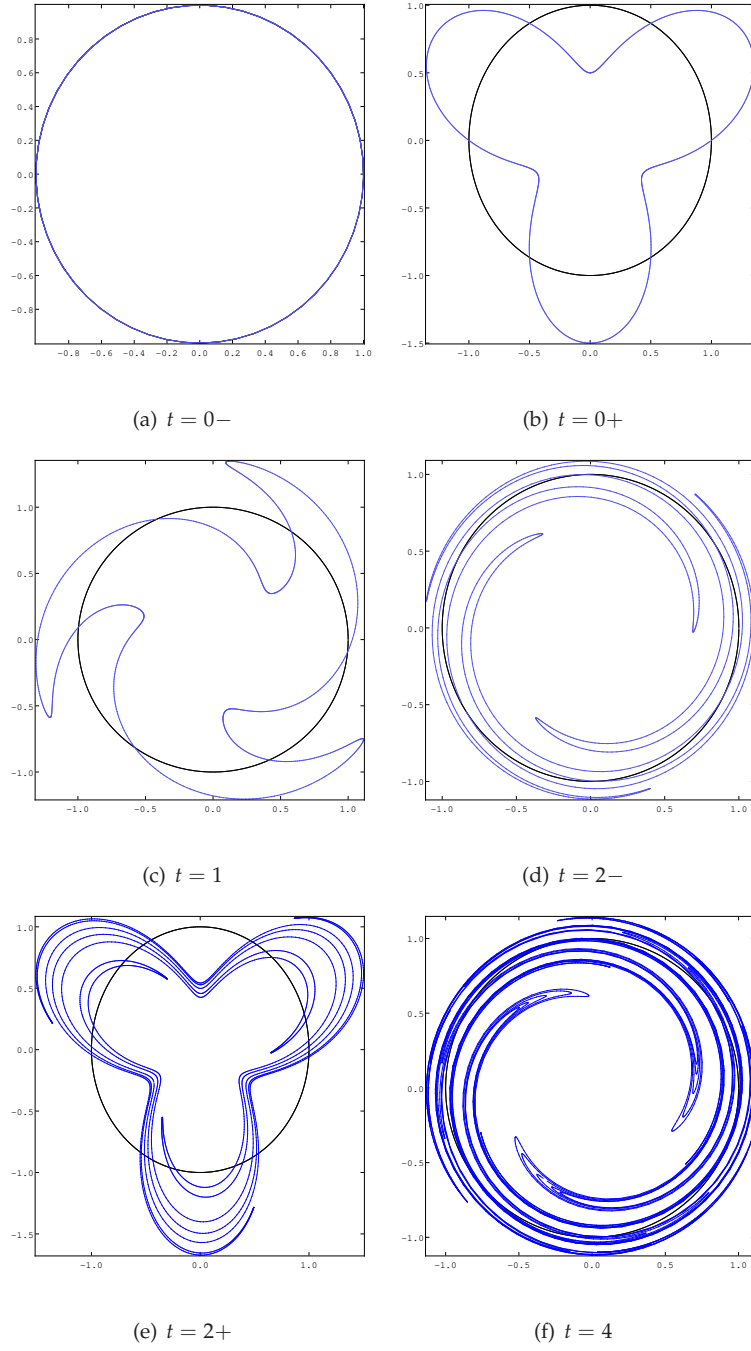


Figure 5: Illustration of the action of kick-and-flow on a continuum of initial conditions placed evenly along the limit cycle. Time indices are for illustrative purpose only. A “-” means before kick, a “+” after.

4 The pulse-driven Hodgkin-Huxley system

This section examines the pulse-driven Hodgkin-Huxley oscillator. After summarizing the numerical results, the distinct response types are related to the properties of the corresponding f_T . The features of f_T specific to the pulse-driven Hodgkin-Huxley system are then explained in terms of the geometry of the Hodgkin-Huxley phase space.

The main numerical results are a characterization of the (T, A) -space using Lyapunov exponents:

$$\begin{aligned} \lambda_{\max} < 0 &\Leftrightarrow F_T \text{ gradient-like} &\Leftrightarrow \text{kicked flow is entrained to input} \\ \lambda_{\max} = 0 &\Leftrightarrow F_T \text{ rotation-like} &\Leftrightarrow \text{kicked flow drifts relative to input} \\ \lambda_{\max} > 0 &\Leftrightarrow F_T \text{ chaotic} &\Leftrightarrow \text{kicked flow is chaotic} \end{aligned}$$

Lyapunov exponents, being asymptotic quantities, cannot detect the presence of transient chaos: when F_T has both a horseshoe and sinks, λ_{\max} will be negative.

The largest Lyapunov exponent λ_{\max} of F_T is easy to compute, for example by pushing forward tangent vectors along orbits. Figure 1 shows λ_{\max} as a function of T , for a few different choices of A . Observe that for values of T which are close to T_γ , λ_{\max} is roughly periodic in T .

Figure 2 replots the results in a more informative way. For each value of A , the fraction of T 's in the interval $[T_\gamma, 8T_\gamma]$ for which $\lambda_{\max}(F_T) > 0$, *etc.*, is computed by sampling from a uniform grid. It is natural to equate these fractions with probabilities because λ_{\max} is roughly a T_γ -periodic function of T , and become more nearly so as $T \rightarrow \infty$. At $A = 10$, the probability of obtaining a positive exponent is roughly 20% and the probability of obtaining a negative exponent is roughly 70%. This roughly means that if one were to pick T randomly out of an interval $[NT_\gamma, (N+1)T_\gamma]$ for large, fixed integer N , then the probability that $\lambda_{\max}(F_T) > 0$ is about 20%.

Figure 2 shows that when A is small, the most likely type of behavior is rotation-like behavior. This possibility becomes less likely as A increases (see Figure 6). At the same time, sinks and chaos both become more likely, with sinks dominating the (T, A) -space.

One feature of Figure 2 specific to the pulse-driven Hodgkin-Huxley flow is that when A is large, the system prefers entrainment over chaos in the sense that entrainment has higher probability. This preference is more pronounced as A increases. This phenomenon is discussed at more length below.

Figure 6 shows some examples of phase resetting curves for the pulse-driven Hodgkin-Huxley system, computed with the numerical method described in the appendix. For sufficiently small values of A , the phase resetting curves are circle diffeomorphisms. The dynamics of f_T is thus rather simple: if there are no fixed points or periodic orbits (and they are unlikely to exist for very small A) then the map is conjugate to a rotation, and the response of the kicked oscillator drifts relative to the phase of the driving pulse train. As A becomes larger, the graph of f_T rather quickly folds over and acquires critical points. The maps remain smooth as long as $K(\gamma) \subset \text{Basin}(\gamma)$.

One striking feature of the graphs in Figure 6 is the “plateau,” a phase interval over which f_T varies very slowly. Another striking feature is the “kink” around $\theta \approx 9.8$. The presence of these features in the graph of f_T is related to the geometry of the Hodgkin-Huxley flow below. But first, let us explore the implications of these features for the dynamics of the kicked oscillator.

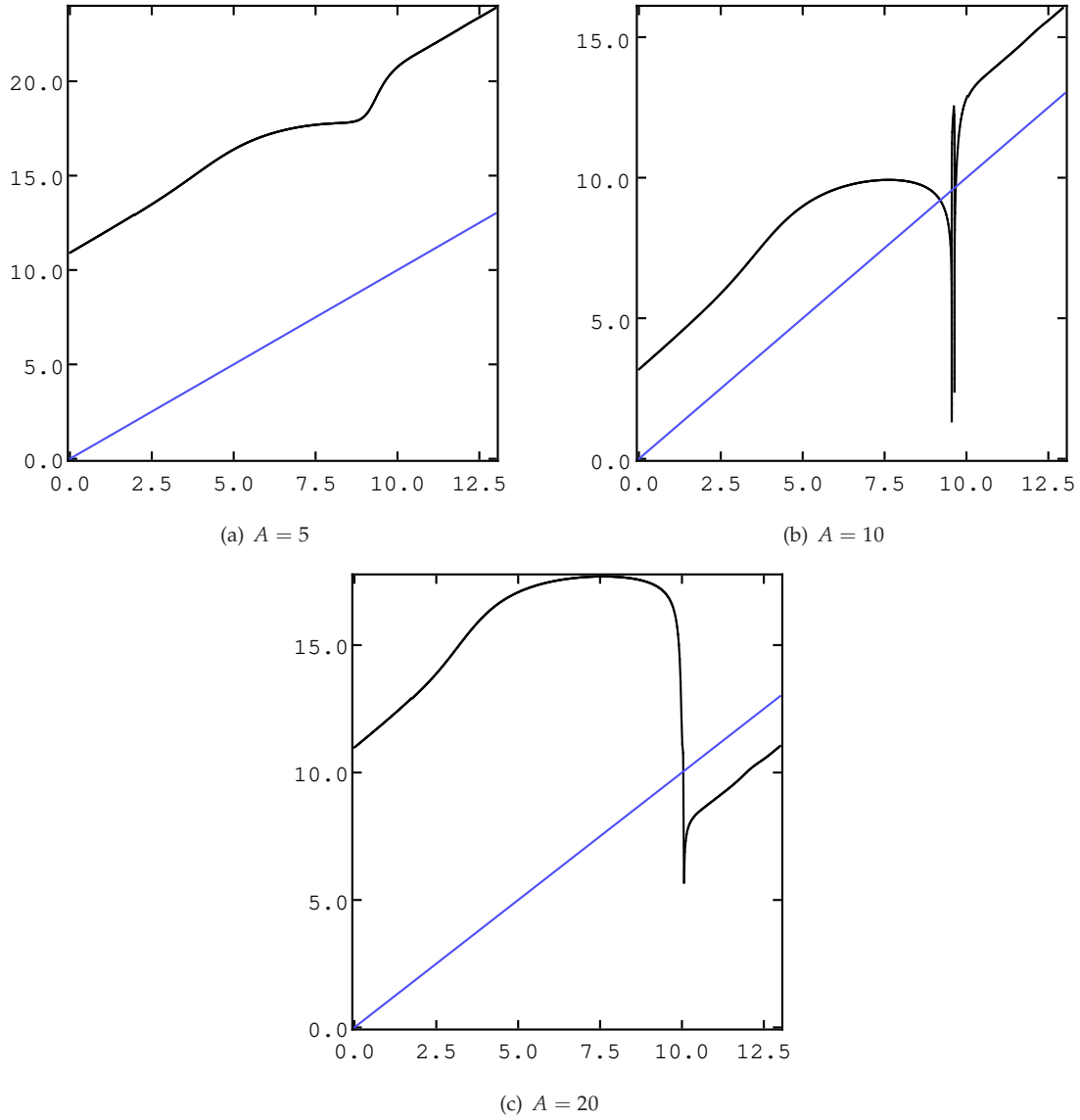


Figure 6: The graph of f_T (actually its lift to a continuous map $\tilde{f}_T : \mathbb{R} \rightarrow \mathbb{R}$) for the pulse-driven Hodgkin-Huxley equations, with (a) $A = 5$, (b) $A = 10$, and (c) $A = 20$. The value of T is immaterial, as varying T would just shift the graph of f_T vertically. Note that f_T has winding number 1 for $A = 5$ and $A = 10$, and has winding number 0 for $A = 20$. The numerical data suggests that the degree changes around $A \approx 13.589$; the precise geometric mechanism is not clear.

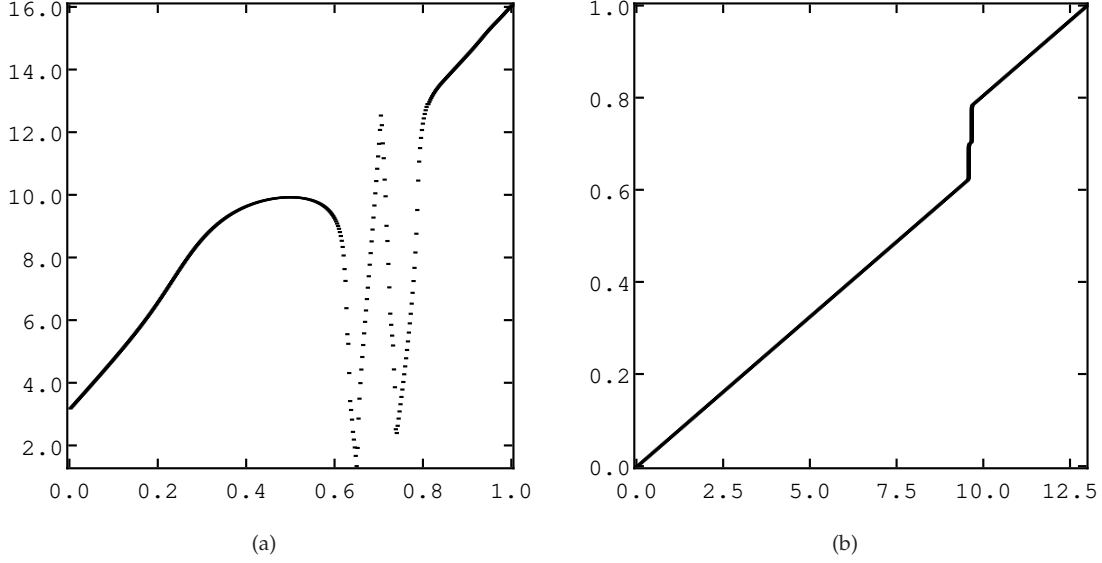


Figure 7: (a) The graph of $f_T \circ g^{-1}$ with drive amplitude $A = 10$, with the abscissa shown in a new coordinate system $\theta' = g(\theta)$ to magnify the region around the “kink.” No interpolation is done in this figure: only actually computed points are shown. (b) The graph of the coordinate transformation g . The map g is generated automatically by the simple adaptive algorithm described in the appendix.

4.1 Entrainment

The plateau provides a simple mechanism for creating sinks: changing the kick period T moves the graph of f_T vertically. Whenever the graph intersects the diagonal with a derivative $|f'_T| < 1$, then a stable fixed point is created.

This mechanism can be used to check the results of Figure 2: compute the graph of the first return map of f_T to an interval around the plateau, then shift the graph vertically using a number of different values of T and estimate the fraction of T 's for which f_T has a stable fixed point (see Figure 8). Table 1 shows the results. For $A = 10$, the 58% probability of sinks corresponds fairly closely with Figure 2. It is unclear whether the “unknown” data in Figure 2 really represent positive or negative Lyapunov exponents. If a significant fraction of those really represent negative exponents, then they represent “small” sinks which are created by some means other than the plateau.

4.2 Chaos

In contrast to the case of sinks, confirming the chaotic behavior of F_T is a more delicate task. Wang-Young theory guarantees the existence of T 's for which F_T is fully chaotic, in the sense that $\lambda_{\max}(F_T) > 0$, correlations decay exponentially fast in time, and F_T possesses an SRB measure, a “physically relevant” invariant measure which captures the behavior of *Lebesgue*-almost every initial condition in a neighborhood of γ and which is smooth along unstable manifolds [30]. However, given a specific value of T , there are no practical, checkable conditions which can guarantee that F_T is chaotic in the sense described above. As explained earlier, the theory only guarantees that the set of T 's for which F_T is chaotic is a set of positive Lebesgue

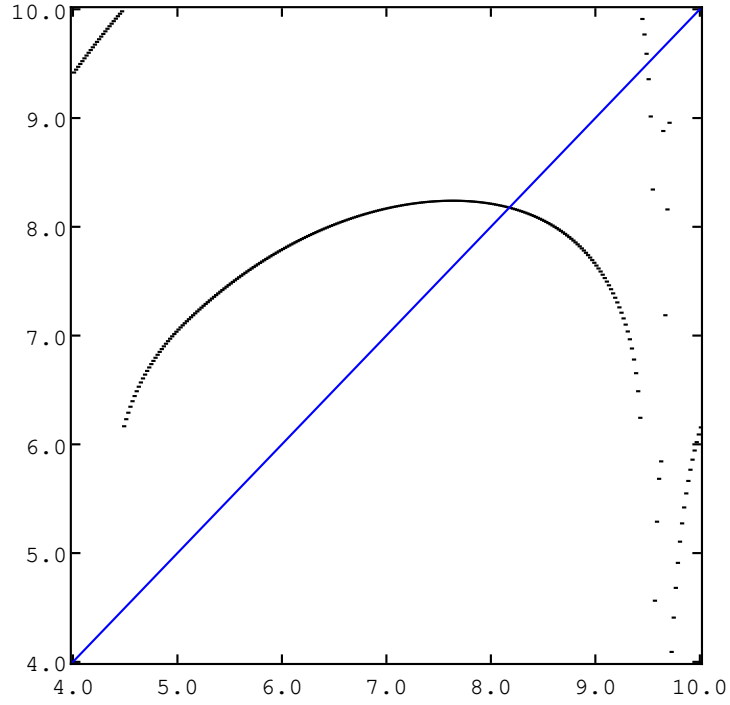


Figure 8: The first return map R_{f_T} to the interval $[4, 10]$ (chosen to enclose the plateau), for $A = 10$ and $T = 17.6$.

Drive amplitude A	Probability of sink near plateau
5	41%
10	58%
20	68%
30	76%

Table 1: Estimates of the probability of obtaining sinks near the plateau, as a function of A . The data for this table is computed by trying about 40 values of T for each choice of A and examining the graph of the first return map to the interval $[4, 10]$ (chosen to coincide with the “plateau”) and its intersection(s) with the diagonal.

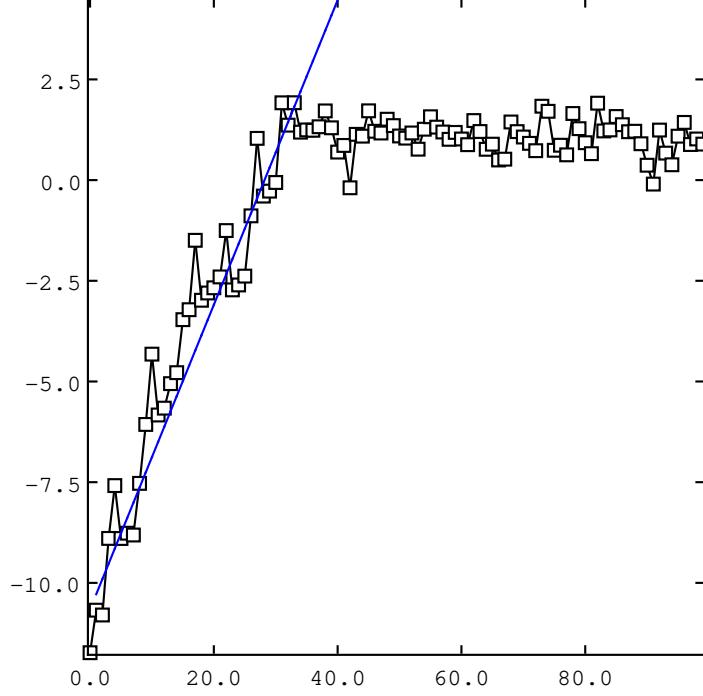


Figure 9: Rate of separation of two nearby F_T -orbits on a \log_{10} scale. Distance is measured in \mathbb{R}^4 . Here, $A = 10$ and $T = 80.8$. The blue line is the best linear fit of the growing part of the distance function; the corresponding exponent is about 0.9. Note that this is significantly larger than the directly-computed (averaged) Lyapunov exponent of 0.57 for these parameters: the exponential separation rate for arbitrarily-chosen starting points does not necessarily reflect the average Lyapunov exponent.

measure and roughly T_γ -periodic; such T 's must be found by other means. An additional complication is that the set of such “chaotic drive periods,” while measurable with positive Lebesgue measure, is not open. Rather than offering computer-assisted proofs of the presence of chaos, the present paper focuses on indirect numerical evidence.

The Lyapunov exponents shown in Figure 1 suggests many promising candidate drive periods T for chaotic behavior, one of which is $A = 10$ and $T = 80.8$. Figure 9 shows the rate of separation of two F_T -orbits with nearby initial conditions at this parameter value. The rate of separation in Figure 9 is about 0.9. The numerically computed Lyapunov exponent for this choice of T and A is ≈ 0.57 . The two differ because the Lyapunov exponent is the exponential separation rate averaged over all initial conditions, weighted by the invariant measure of F_T . Figure 10 shows the graph of f_T and its iterate f_T^2 . As can be seen, neither f_T nor f_T^2 has a stable fixed point, hence any sinks which are present must have period ≥ 3 . Figure 11 shows the correlation function $C_{vv}(n)$ for F_T : it appears to be decaying, although the data is insufficient for concluding whether the decay is exponential. This is again consistent with Wang-Young theory: when F_T is exponentially mixing, the rate of decay is expected to be quite slow.

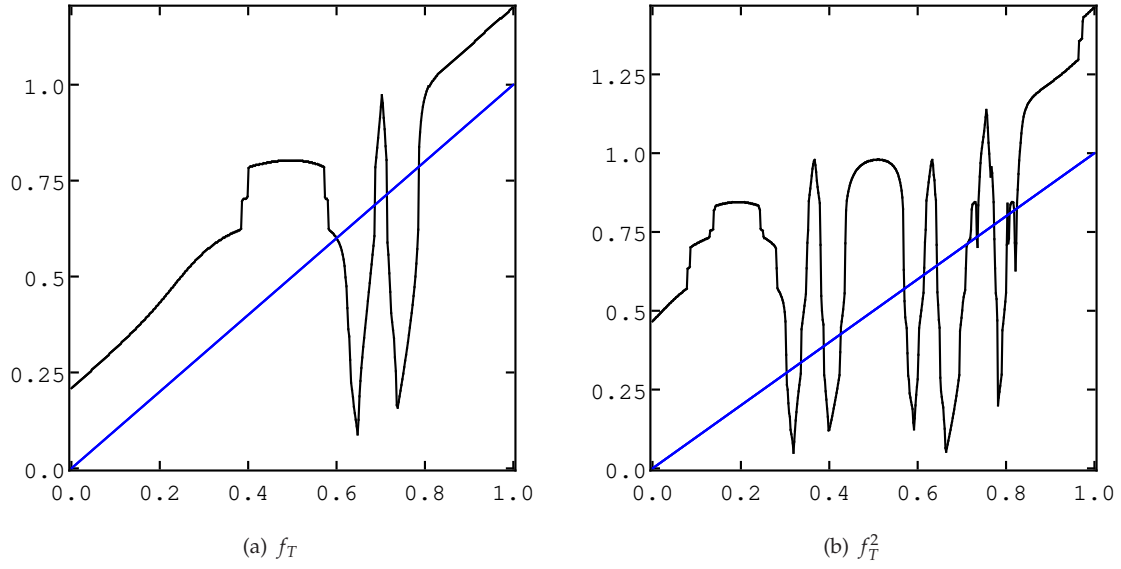


Figure 10: Graph of $g \circ f_T \circ g^{-1}$ and its iterate $g \circ f_T^2 \circ g^{-1}$, for $A = 10$ and $T = 80.8$. As in Figure 7, the graphs are shown in an adaptively generated coordinate system g .

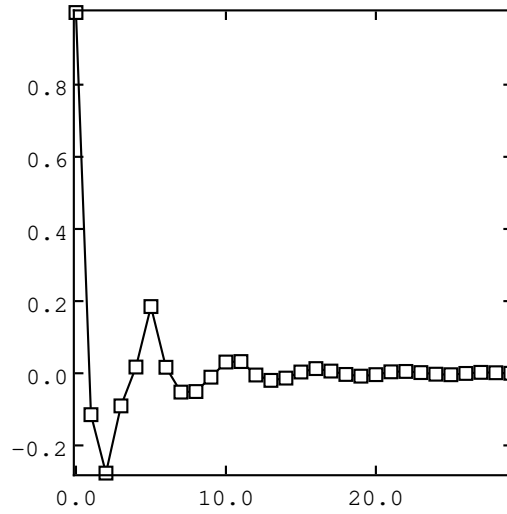


Figure 11: Normalized autocorrelation function $C_{vv}(n)$ for the v variable of the time- T map F_T . This graph appears to indicate that the dynamics is mixing, but the data is insufficient for determining whether or not the system is exponentially mixing.

4.3 Horseshoes & transient chaos

Wang-Young theory also guarantees the existence of T 's for which F_T exhibits transient chaos, *i.e.* F_T possesses a horseshoe, an invariant Cantor set on which F_T is uniformly hyperbolic. Because of its invariance, an orbit which gets close to a horseshoe will return a number of times before “escaping.” Because of the uniform hyperbolicity, a pair of nearby orbits entering the horseshoe will separate exponentially by the time they both escape.

The coexistence of a horseshoe with a sink produces transient chaos in the following way: almost every F_T -orbit would eventually fall into a sink, but as an orbit nears a horseshoe it would dance around unpredictably for a finite number of iterations. Two nearby orbits which enter the vicinity of a horseshoe can emerge widely separated, and hence entrain to the input pulse train *out of phase*. In terms of time series data, this kind of behavior can be recognized by looking at *pairs* of trajectories and finding that they chaotically “flutter” about before settling down into a steady periodic motion, likely out of phase.

In contrast to entrainment and chaos, transient chaotic behavior is difficult to observe in the pulse-driven Hodgkin-Huxley system. The associated expansion rates are so large that most trajectories entering a neighborhood of the horseshoe escape after a few iterates of F_T . Nevertheless, it is interesting to find horseshoes in the pulse-driven Hodgkin-Huxley model, as their presence is predicted by Wang-Young theory.

To provide numerical evidence for the existence of horseshoes, one first looks for an interval $I \subset [0, T_\gamma)$ such that $f_T(I)$ gets mapped completely across I at least twice. It is easy, for example, to find a “small” horseshoe around the kink in the phase resetting curve. See Figure 12. The phase interval I tells us the rough location of a horseshoe for F_T . To go from such an interval I to a horseshoe for the full map F_T , it is necessary to (i) blow up the corresponding segment of γ to form an open set $U \subset \mathbb{R}^4$ such that $F_T(U)$ intersects U at least twice, and the intersection stretches all the way across U in the unstable direction (along γ); and (ii) find invariant cones [11]. This can be done in a straightforward but tedious manner.

4.4 Plateau & kink

The presence of the plateau and the kink in f_T can be explained in terms of the phase space structure of the Hodgkin-Huxley flow. The plateau exists because of two properties of the Hodgkin-Huxley flow near γ . First, the speed along γ is extremely uneven, with most of the fast “action” concentrated in a small amount of time (= phase). Second, a short segment $\tilde{\gamma}$ of γ which lies in the relatively slow part of the limit cycle, when kicked, becomes (nearly) parallel to a W_{ss} -leaf. Because the segment $\tilde{\gamma}$ lies in a relatively slow part of the cycle, it corresponds to a long phase interval. Because $K(\tilde{\gamma})$ is nearly parallel to a W_{ss} -leaf, the map f_T varies only very slowly over this phase interval.

These claims can be checked by examining the various factors which contribute to the derivative f'_T . To begin, since changing T amounts to shifting the graph of f_T , it has no impact on f'_T . So it suffices to consider $f = f_0$, which satisfies

$$\gamma \circ f = \pi_{ss} \circ K \circ \gamma. \quad (10)$$

Thus the map f is a composition of γ (and γ^{-1}), which act as changes of coordinates from the phase variable $\theta \in [0, T_\gamma)$ to \mathbb{R}^4 , and a geometric part $\pi_{ss} \circ K$. The geometric part $\pi_{ss} \circ K$ has derivative $D(\pi_{ss} \circ K) = (D\pi_{ss} \circ K) \cdot DK = D\pi_{ss} \circ K$; $DK = \text{Id}$ because K is a translation. The projection map π_{ss} maps the basin of γ (a 4-dimensional object) onto γ (a 1-dimensional object), so $D\pi_{ss}$ must be a matrix of rank ≤ 1 . For any $x \in \gamma$, then, one can write

$$D\pi_{ss}(x) = \sigma(x) \cdot [u(x) \otimes v(x)], \quad (11)$$

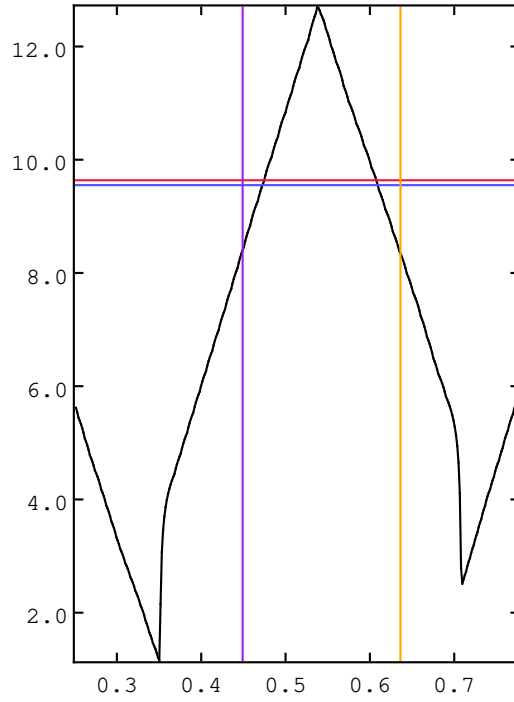


Figure 12: The phase resetting map and an interval I (marked by the straight lines) which maps across itself twice. The abscissa (but not the ordinate) is shown in transformed coordinates. Here, $A = 10$ and $T = 81$. This is a “small” horseshoe: because the derivative of f_T is so large there (on the order of $10^3 \sim 10^4$), most numerically computed orbits escape the horseshoe after a few iterates.

where u and v are unit vectors and σ is a nonnegative scalar. This factorization has the following geometric interpretation: let x denote a point on the limit cycle, $y = K(x)$ the image of x after the kick, and $z = \pi_{ss}(y)$ the image of x under $\pi_{ss} \circ K$. Then $D(\pi_{ss} \circ K)(x) = \sigma(y) \cdot [u(y) \otimes v(y)]$. It is straightforward to check that the unit vector $v(y)$ is normal to $W_{ss}(z)$ at y , the unit vector $u(y)$ is tangent to γ at z , and the scalar $\sigma(y)$ measures the amount by which the strong-stable foliation “spreads” along γ as one moves in a direction normal to $W_{ss}(z)$ at y .

Going back to the expression for f' , a simple calculation shows that

$$f' = \frac{(\sigma \circ K \circ \gamma) \cdot \langle v \circ K \circ \gamma, \hat{\gamma} \rangle \cdot |\gamma'|}{|\gamma' \circ f|}, \quad (12)$$

where $\hat{\gamma}$ is $\gamma' / |\gamma'|$. The factors $|\gamma'|$ and $|\gamma' \circ f|$ relate phase to arclength. The inner product $\langle v \circ K \circ \gamma, \hat{\gamma} \rangle$ gives the angle between $K(\gamma)$ and $W_{ss}(z)$ at y . These quantities are easy to compute numerically (see below) and are shown in Figure 13. As can be seen, the critical point in f corresponds to the vanishing of $\langle v \circ K \circ \gamma, \hat{\gamma} \rangle$, i.e. the kicked segment becomes tangent to a W_{ss} manifold at the plateau.

Remark 4.1. To numerically compute $D(\pi_{ss} \circ K) = D\pi_{ss} \circ K$, fix $x \in \gamma$ and compute $D\Phi_{T_\gamma}^n(K(x))$ for $n = 1, 2, 3, \dots$. When the matrix has converged up to some given accuracy, compute its singular value decomposition. The singular values should consist of a dominant singular value σ_1 and 3 nearly zero singular values σ_2, σ_3 , and σ_4 . The nearly zero $\sigma_i \rightarrow 0$ as $n \rightarrow \infty$. The dominant singular value σ_1 is an approximation of σ , while the left and right singular vectors are the vectors u and v . Note that this computation requires a relatively accurate estimate of T_γ , without which the computation would not converge. This paper adopts the following strategy: instead of estimating T_γ just once and reusing its value, solve the system

$$\begin{aligned} \dot{x}_1 &= H(x_1) \\ \dot{x}_2 &= H(x_2) \\ \dot{J} &= DH(x_2) \cdot J \end{aligned}$$

where H is the Hodgkin-Huxley flow field, $x_1(0) \in \gamma$, $x_2(0) = K(x)$ (where x is the point at which we would like to evaluate $D(\pi_{ss}(K(x)))$), and J is an 4×4 matrix with $J(0) = \text{Id}$. The reference trajectory x_1 is used to count the number of periods which have elapsed, and the trajectory (x_2, J) is used to compute $D(\pi_{ss}(K(x)))$. This appears to work fairly well in practice.

Note that the numerical results of Figure 13 only shows that the kicked segment becomes tangent to the strong-stable manifolds. They do not explain why the tangency is so persistent as A increases. An answer to this question would necessarily involve a more detailed analysis of the geometry of the strong-stable foliation of γ .

As for the kink, it is natural to suspect that the map f_T in Figure 6, for $A = 10$ or $A = 20$, is discontinuous around kink. Such a discontinuity would indicate that $K(\gamma)$ intersects the complement of the basin of γ . This is not likely the case: the continuity of f_T is strongly suggested by the convergence of the adaptive algorithm described in the appendix, which computes the graph of f_T on an automatically generated grid $\{\theta_n\}$, refining the grid until $|f_T(\theta_{n+1}) - f_T(\theta_n)| \leq \delta$. In Figure 7, the tolerance parameter δ is set to 0.1. Empirically, the algorithm still converges when δ is reduced further.

The kink is likely caused by a segment of γ being kicked near the stable manifold of the unstable fixed point. This causes the segment to wind around the stable manifold and eventually spirals away from the

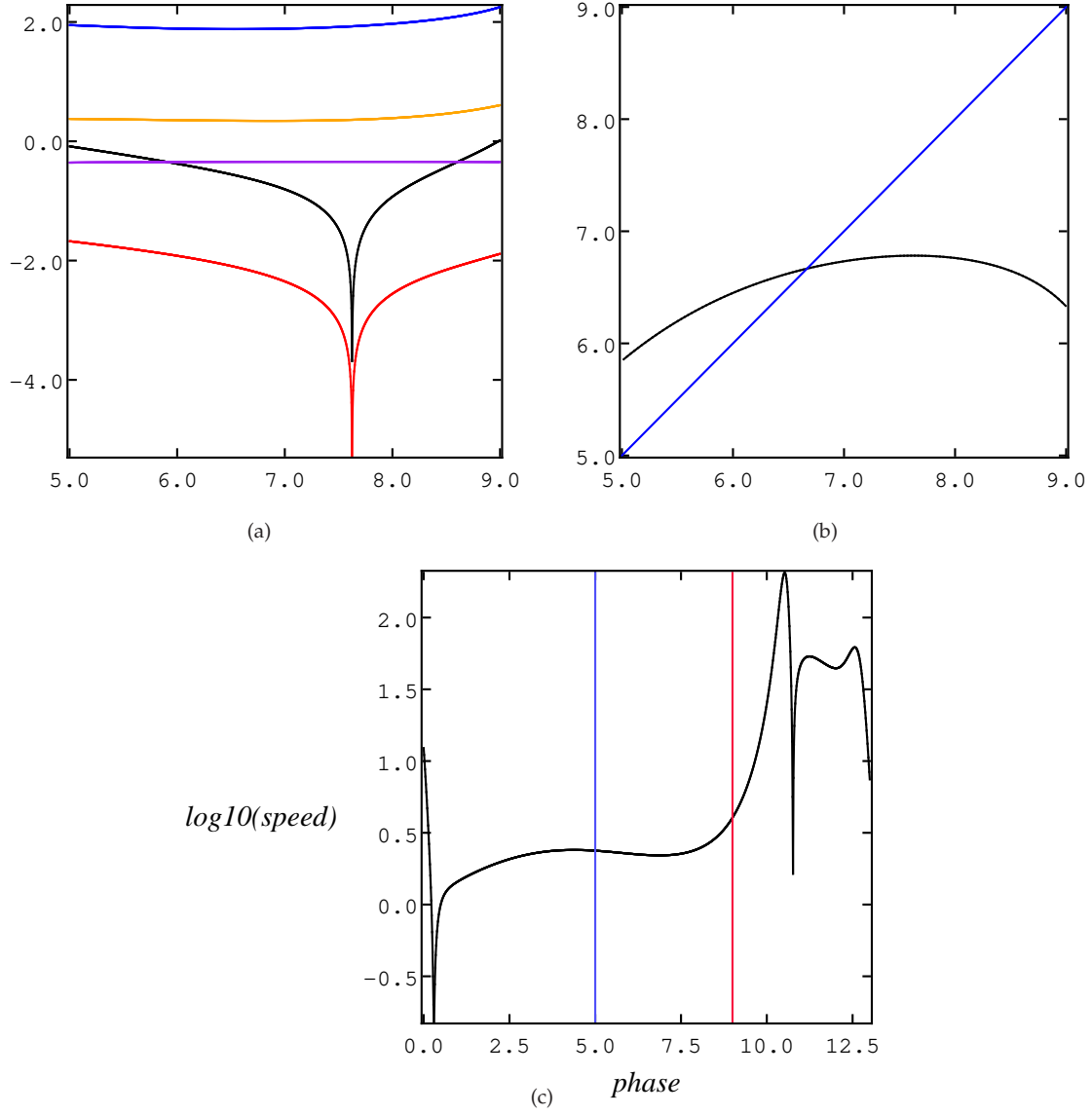


Figure 13: The origin of the plateau: in (a), the curves are (i) *Black*: $\log_{10} |f'|$; (ii) *Blue*: $\log_{10} \sigma$; (iii) *Red*: $\log_{10} |\langle \gamma', v \rangle|$; (iv) *Purple*: $-\log_{10} |\gamma' \circ f|$; (v) *Orange*: $\log_{10} |\gamma'|$. In (b), the graph of f_T near the plateau is shown over for reference. Here, $A = 10$. (c) The speed of the Hodgkin-Huxley flow along γ . The vertical lines mark the interval $[5, 9]$, which is part of the plateau.

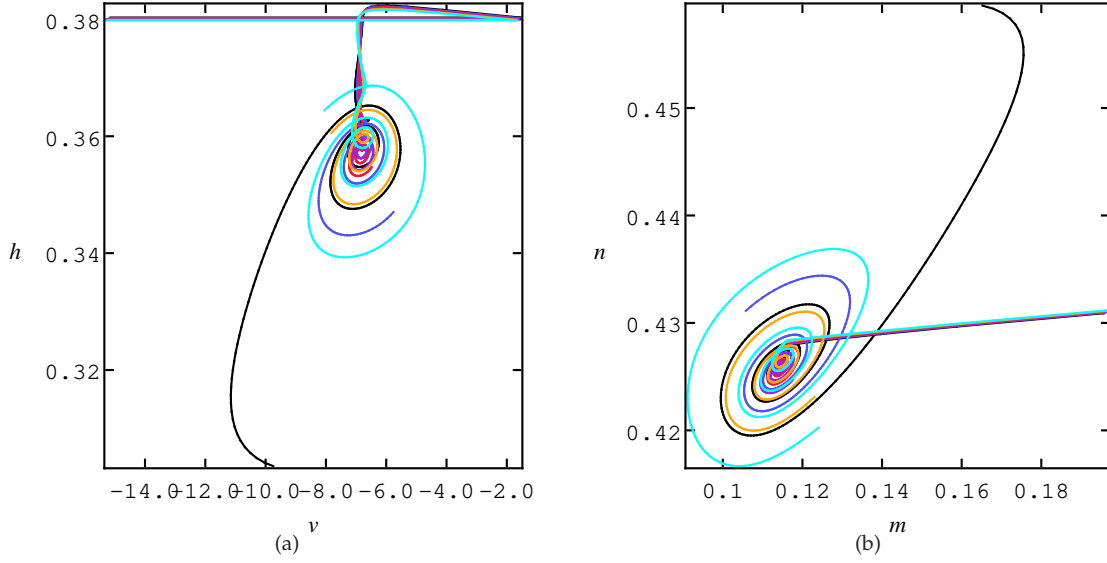


Figure 14: A potentially misleading but suggestive picture: in (a), a segment of γ , starting in the upper left corner of the picture, is kicked straight across to the upper right corner. It is then allowed to flow, and finds its way toward the fixed point before eventually spiraling away. The overall direction of motion is from top to bottom. (b) Another view of the approach to the fixed point. The overall direction of motion here is from right to left. The kick amplitude is $A = 13.589$.

fixed point. (Recall that the two unstable eigenvalues of the fixed point form a complex conjugate pair.) In the process the kicked segment spreads apart and its subsets pick up different amounts of time delays. This scenario is suggested by Figure 14. However, Figure 14, while suggestive, is really misleading because the Hodgkin-Huxley flow takes place in \mathbb{R}^4 , not \mathbb{R}^3 , so a projection into 2 dimensions is inappropriate. A more careful test of this claim is to try to isolate a critical kick amplitude A_{crit} at which $K(\gamma)$ intersects the stable manifold of the fixed point, and to compute the phase resetting curves for a sequence of values of A around A_{crit} . This has been done: using the Nelder-Mead algorithm [19] to minimize the closest distance to the fixed point, one such critical value A_{crit} has been determined to be $\approx 13.58953\dots$ When $A = A_{\text{crit}}$ exactly, f_T should wind around infinitely many times and possess a singularity near the location(s) of intersection. For $A \neq A_{\text{crit}}$, f_T remains smooth, but as $A \rightarrow A_{\text{crit}}$ the winding number of f_T should blow up. This is shown in Figure 15.

4.5 Response to finite-duration pulses

A natural variation on the numerical experiments of previous sections is to replace instantaneous impulses with finite-duration pulses. Heuristically, if the pulse duration t_0 is less than the fastest of the intrinsic timescales of γ , the resulting response should be essentially the same as the response to instantaneous impulses. With $I = -14.2211827403$, these time scales are 12.944 (= the period), 5.1, 0.50, and 0.12 (corresponding to the negative Lyapunov exponents).

Figure 16 summarizes the numerical results for $t_0 = 0.05$ (shorter than all time scales), 0.3 (shorter than all but one time scale), 2.75 (shorter than all but two fastest time scales), and 9.0 (very slow, not really

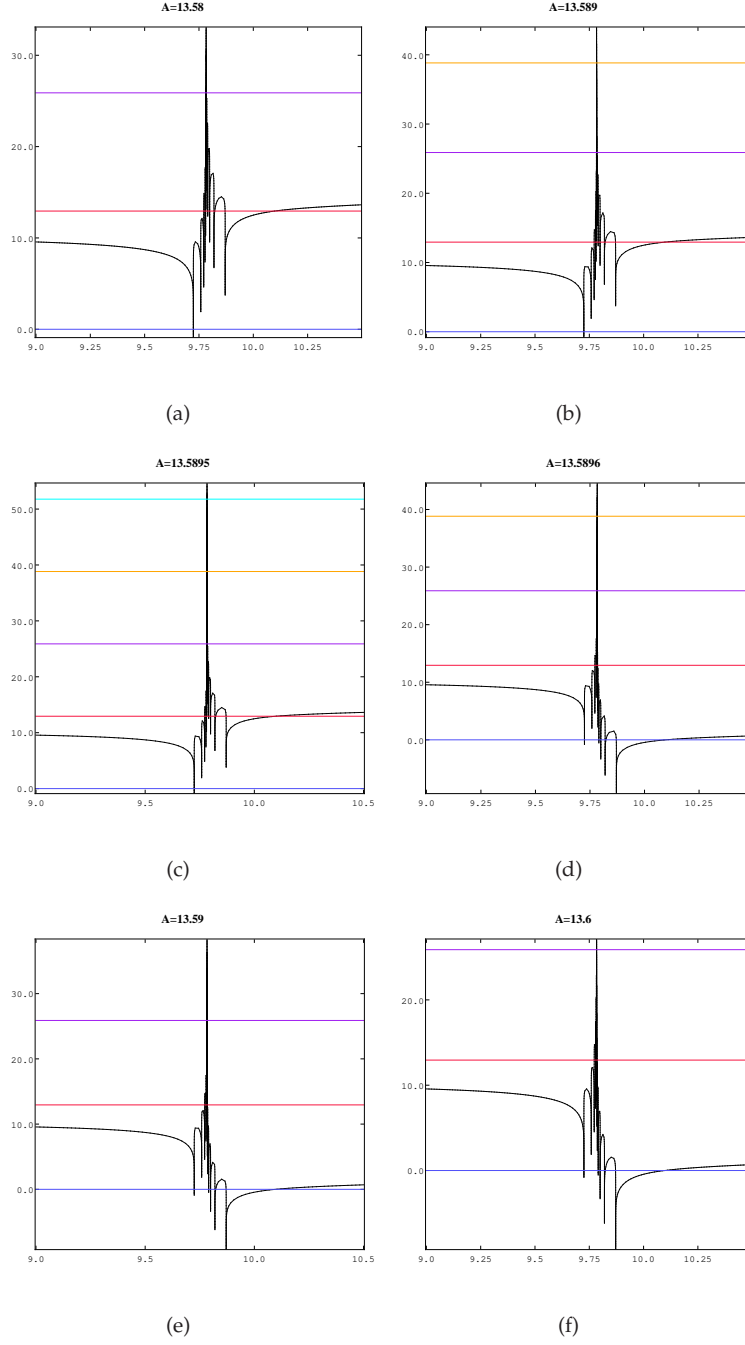


Figure 15: Graphs of f_T for kick amplitudes A approaching A_{crit} from below (a-c) and above (d-f). The horizontal lines mark integral multiples of T_γ .

pulsatile in any sense of the word). These graphs should be compared to Figure 2. The pulse amplitude is adjusted so that the *total* amount of charge delivered is the same as an impulse of amplitude A . Interestingly enough, the behavior seen earlier impulses are quite robust and disappear only when $t_0 = 9$. These results suggest that the contracting directions do not mix very much over γ , and only the slowest contracting time scale participates in the production of chaotic behavior.

5 Conclusions & future work

The results reported here have shown that the pulse-driven Hodgkin-Huxley model responds to low-frequency periodic impulse forcing in a surprisingly wide range of ways. Depending on the drive period and drive amplitude, the response can range from entrainment to fully chaotic behavior. This is consistent with the predictions of Wang-Young theory for the Hodgkin-Huxley oscillator. Furthermore, it is relatively straightforward to arrive at mathematically plausible explanations of the special features of this system using a combination of geometric reasoning and computation.

From the point of view of neuronal models, one slightly unrealistic feature of the pulse-driven Hodgkin-Huxley model studied here is the use of low-frequency periodic impulse trains as forcing terms. While impulses are frequently used to model the *output* of neurons, for example in integrate-and-fire models, the typical input to a single neuron may not look like a low-frequency impulse train at all because of large “fan-in.” Recent theoretical studies of neural reliability favor stationary gaussian processes with higher frequency components (or Poisson point processes with high arrival rates) as model inputs. However, the low-frequency pulsatile inputs studied here may provide a model for artificial, externally-applied electrical stimuli. Single-neuron and small network models with pulsatile stimuli have acquired some interest in recent years as theoretical testbeds for electrical stimulation techniques which suppress epileptic seizures [7, 23].

This paper focuses on a single neuron for simplicity, but Wang-Young theory may apply to neuronal network models with intrinsic oscillatory behavior. Such networks may be of more direct scientific interest, and it would be natural to explore the dynamical behavior predicted by Wang and Young and their consequences for interacting networks of neurons. For a population of uncoupled (or very weakly coupled), nearly identical Hodgkin-Huxley neurons, all experiencing the same external forcing but starting with different initial conditions, the results presented here have the following consequences: if the kick time T is such that a sink exists, then the population will entrain to the input pulse train, and hence to each other (albeit possibly out of phase, unless the sink is a fixed point). The distinct phases subdivides the population into a finite number of subpopulations. If the kick time T is such that a horseshoe coexists with a sink, then even neurons with nearby initial conditions can entrain to the input pulse train out of phase. If T is chosen to guarantee the existence of a strange attractor, then the phases of the neurons will be uncorrelated with each other.

An interesting mathematical question is whether all the phenomena described here survive when one allows for the drive parameters A and T to vary randomly from spike to spike, for example using a Poisson process to generate random kick times. It is not immediately obvious what conditions are needed to guarantee that the resulting random Lyapunov exponent is positive, for example.

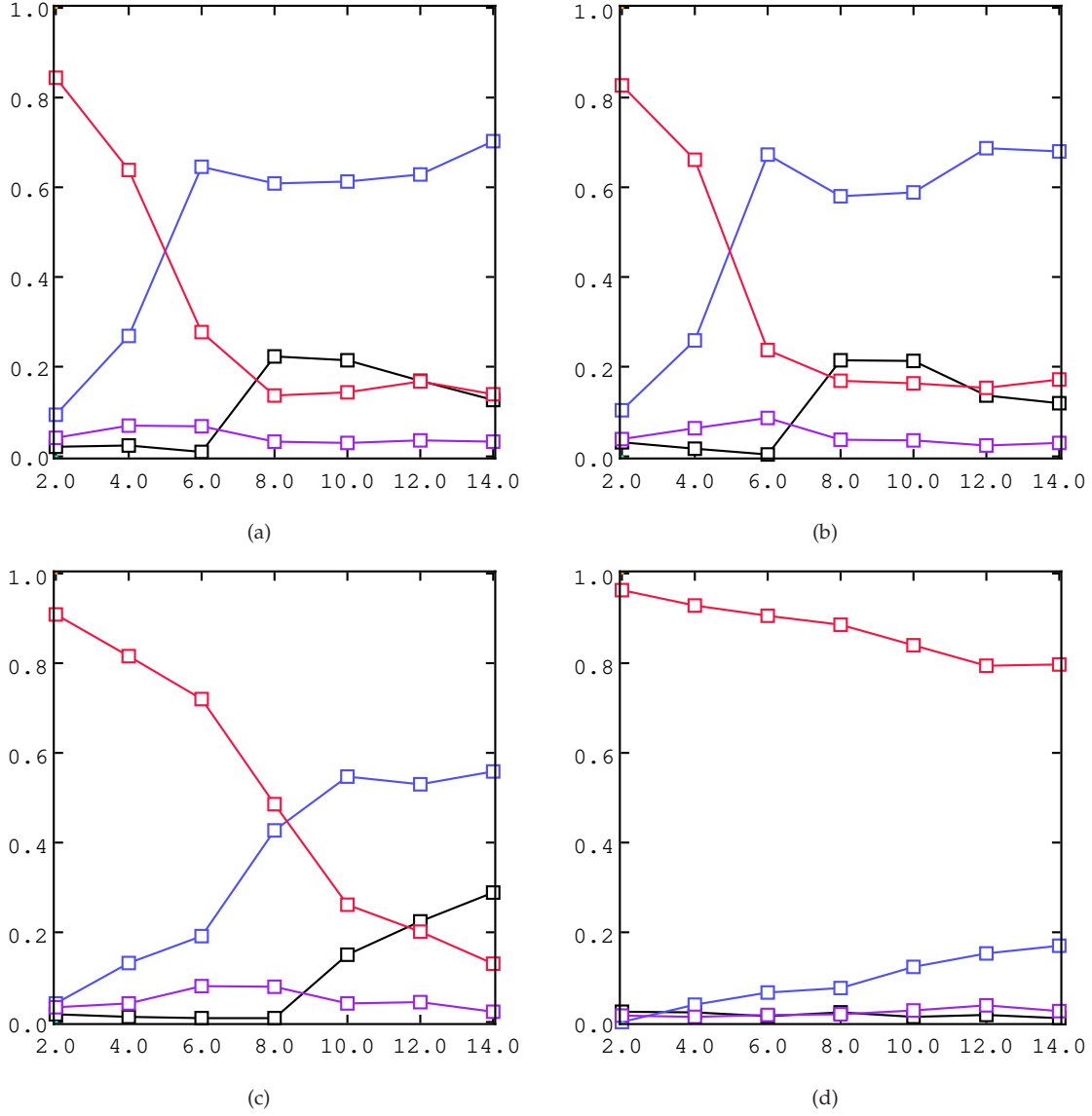


Figure 16: Distribution of Lyapunov exponents for $I = -14.2211827403$ with finite-duration pulse of duration (a) $t_0 = 0.05$, (b) $t_0 = 0.3$, (c) $t_0 = 2.75$, and (d) $t_0 = 9.0$. See Figure 2 caption for details. Recall that the Lyapunov exponents of the unperturbed limit cycle γ are -0.196 , -2.01 , and -8.31 , corresponding to relaxation times of 5.1, 0.50, and 0.12.

Appendix: Computation of phase resetting curves

A simple algorithm, due to Ermentrout and Kopell [9] (see also Appendix A in [4]), facilitates the efficient computation of phase resetting curves. The present paper uses the variant described below.

Note that this method is somewhat less flexible than applying shooting methods to the two-point boundary value problem formulation of [9]. But it may have the advantage of numerical stability and ease of implementation in higher dimensional problems, particularly in infinite-dimensional systems such as reaction-diffusion equations.

Algorithm (Phase resetting curves via stable subspaces).

1. Estimate the period T_γ of the limit cycle γ by numerically solving the unforced equations starting with a point on or near γ .
2. Discretize γ by subdividing the time interval $[0, T_\gamma)$ into N intervals and computing the corresponding points $x_i \in \gamma$. Fix an arbitrary reference point x_0 on γ so that each point on γ can be assigned a unique phase $\theta \in [0, T_\gamma)$.
3. For each point x_i computed in the previous step, compute the Jacobian $DH(x_i)$ of the Hodgkin-Huxley flow field H at that point.
4. Using the results of the previous two steps, solve

$$\begin{aligned}\dot{x} &= -H(x), \\ \dot{\xi} &= \eta - \langle \eta, \xi \rangle \xi, \\ \eta &= DH(x)^T \xi,\end{aligned}\tag{13}$$

using the grid points $\{x_i\}$ computed in the previous steps. The \dot{x} part of the equation above is clearly numerically unstable, but that is not a problem because we have already have a numerical representation of γ .

The equations above are a variant of the usual method for computing Lyapunov exponents [11]. They preserve the length of $\xi(t)$, though in practice, it is necessary to rescale $\xi(t)$ to ensure that this constraint is maintained. As $t \rightarrow \infty$, $\xi(t)$ becomes orthogonal to the strong-stable linear subspace $E_{ss}(x(t))$ of γ . The subspace $E_{ss}(x(t))$ is tangent to the strong-stable manifold $W_{ss}(x(t))$ at $x(t)$.⁴

5. Using Equation (8) in combination with the linear subspaces computed in the previous step, we can now approximate the phase resetting curve. Start with a point $x \in \gamma$ and compute $\Phi_t(K(x))$ for increasing t . Let $t_0 > 0$ be the minimum positive time at which $\Phi_{t_0}(K(x))$ has (i) returned to a small, fixed neighborhood of γ (in this paper this is chosen to be a neighborhood of distance 10^{-4} around

⁴These equations can be generalized to the following:

$$\begin{aligned}\dot{x} &= -H(x) \\ \dot{\xi}_i &= \eta_i - \langle \eta_i, \xi_i \rangle \xi_i - \sum_{j < i} (\langle \xi_i, \dot{\xi}_j \rangle + \langle \eta_i, \xi_j \rangle) \xi_j \\ \eta_i &= DH(x)^T \xi_i\end{aligned}\tag{14}$$

If the vectors (ξ_i) form an orthonormal basis at $t = 0$, then the equations will guarantee that $(\xi_i(t))$ are orthonormal for all $t > 0$. Again, it will be necessary to perform Gram-Schmidt orthogonalizations periodically to maintain this constraint. The vector $\xi_1(t)$, as before, converges to a vector orthogonal to $E_{ss}(x(t))$. So $(\xi_2(t), \xi_3(t), \xi_4(t))$ span $E_{ss}(x(t))$. Similarly, the vectors $(\xi_3(t), \xi_4(t))$ span the subspace consisting of the 2 fastest contracting directions, and $(\xi_4(t))$ spans the fastest contracting direction.

γ); and (ii) $\Phi_{t_0}(K(x))$ lies within one of the pre-computed linear subspaces $E_{ss}(x_*)$ for some point x_* . Let θ_* denote the phase of the point x_* . Then the new phase of the system is $(T + \theta_* - t_0) \pmod{T_\gamma}$.

6. Proceed to the next grid point and repeat.
7. When the derivative of the phase resetting curve becomes large or infinite, it may be necessary to adaptively generate the grid points on which the curve is evaluated. Generally speaking, the grid $\{x_i\}$ constructed in Step 2 need not equal the grid $\{x'_i\}$ on which the phase resetting curve is evaluated. In particular, the grid $\{x'_i\}$ can be adaptively chosen to ensure that $|\hat{f}_a(x'_{i+1}) - \hat{f}_a(x'_i)| \leq \epsilon$, where \hat{f}_a denotes the computed phase resetting curve and ϵ is a fixed number, in this paper usually 0.1. This adaptive mechanism provides a way to detect discontinuities in f_T .

Acknowledgements

I am grateful to Lai-Sang Young for her generous help with this work. It is also a pleasure to thank Eric Shea-Brown, Charles Peskin, John Rinzel, and Louis Tao for many helpful and stimulating conversations, and for references to prior work on this subject. This work was supported by a Mathematical Sciences Postdoctoral Fellowship from the National Science Foundation.

References

- [1] K. AIHARA AND G. MATSUMOTO, *Chaotic oscillations and bifurcations in squid giant axons*, in *Chaos, Nonlinear Science: Theory and Applications*, Manchester University Press, 1986.
- [2] M. BENEDICKS AND L. CARLESON, *The dynamics of the Hénon map*, *Annals of Mathematics*, 133 (1991).
- [3] E. N. BEST, *Null space in the Hodgkin-Huxley equations: a critical test*, *Biophysical Journal*, 27 (1979), pp. 87–104.
- [4] E. BROWN, J. MOEHLIS, AND P. HOLMES, *On the phase reduction and response dynamics of neural oscillator populations*, *Neural Computation*, 16 (2004), pp. 673–715.
- [5] J. CRONIN, *Mathematical Aspects of Hodgkin-Huxley Neural Theory*, Cambridge University Press, 1987.
- [6] S. DOI AND S. SATO, *The global bifurcation structure of the bvp neuronal model driven by periodic pulse trains*, *Mathematical Biosciences*, 125 (1995), pp. 229–250.
- [7] D. M. DURAND AND M. BIKSON, *Suppression and control of epileptiform activity by electrical stimulation: a review*, *Proceedings of the IEEE*, 89 (2001), pp. 1065–1082.
- [8] G. B. ERMENTROUT, *Simulating, Analyzing, and Animating Dynamical Systems: A Guide to XPPAUT for Researchers and Students*, vol. 14 of *Software, Environments, and Tools*, SIAM, 2002.
- [9] G. B. ERMENTROUT AND N. KOPELL, *Multiple pulse interactions and averaging in systems of coupled neural oscillators*, *Journal of Mathematical Biology*, 29 (1991), pp. 195–217.
- [10] L. GLASS AND M. C. MACKEY, *From Clocks to Chaos: The Rhythms of Life*, Princeton University Press, 1988.

- [11] J. GUCKENHEIMER AND P. HOLMES, *Nonlinear Oscillations, Dynamical Systems, and Bifurcations of Vector Fields*, Springer-Verlag, 1983.
- [12] J. GUCKENHEIMER AND R. OLIVA, *Chaos in the Hodgkin-Huxley model*, SIAM Journal on Applied Dynamical Systems, 1 (2002), pp. 105–114.
- [13] A. L. HODGKIN AND A. F. HUXLEY, *A quantitative description of membrane current and its application to conduction and excitation in nerve*, Journal of Physiology, 117 (1952), pp. 500–544.
- [14] A. KATOK AND B. HASSELBLATT, *Introduction to the Modern Theory of Dynamical Systems*, Cambridge University Press, 1995.
- [15] M. LEVI, *Qualitative analysis of periodically forced relaxation oscillations*, Memoirs of the American Mathematical Society, 214 (1981), pp. 1–147.
- [16] N. LEVINSON, *A second order differential equation with singular solutions*, Annals of Mathematics, 50 (1949), pp. 127–153.
- [17] A. OKSASOGLU AND Q. WANG, *Strange attractors in periodically-kicked Chua's circuit*, International Journal of Bifurcation and Chaos, (to appear).
- [18] A. S. PIKOVASKY AND J. KURTHS, *Coherence resonance in a noise-driven excitable system*, Physical Review Letters, 78 (1996), pp. 775–778.
- [19] W. H. PRESS, B. P. FLANNERY, S. A. TEUKOLSKY, AND W. T. VETTERLING, *Numerical Recipes in C*, Cambridge University Press, 1992.
- [20] J. RINZEL AND G. B. ERMENTROUT, *Analysis of neural excitability and oscillations*, in *Methods in Neuronal Modelling: From Synapses to Networks*, MIT Press, 1989.
- [21] S. SMALE, *Differential dynamical systems*, Bulletin of the American Mathematical Society, 73 (1967), pp. 747–817.
- [22] T. TAKABE, K. AIHARA, AND G. MATSUMOTO, *Response characteristics of the Hodgkin-Huxley equations to pulse-train stimulation*, Transactions of IEICE Japan (Japanese edition), J71-A (1988), pp. 744–750.
- [23] P. A. TASS, *Effective desynchronization with a resetting pulse train followed by a single pulse*, Europhysics Letters, 55 (2001), pp. 171–177.
- [24] B. VAN DER POL AND J. VAN DER MARK, *Frequency demultiplication*, Nature, 120 (1927), pp. 363–364.
- [25] Q. WANG AND L.-S. YOUNG, *Strange attractors with one direction of instability*, Communications in Mathematical Physics, 218 (2001).
- [26] ———, *From invariant curves to strange attractors*, Communications in Mathematical Physics, 225 (2002).
- [27] ———, *Strange attractors in periodically-kicked limit cycles and Hopf bifurcations*, Communications in Mathematical Physics, 240 (2003).
- [28] ———, *Toward a theory of rank-1 attractors*, preprint, (2004).
- [29] A. WINFREE, *The Geometry of Biological Time, Second Edition*, Springer-Verlag, 2000.

- [30] L.-S. YOUNG, *Ergodic theory of differentiable dynamical systems*, in Real and Complex Dynamics, NATO ASI Series, Kluwer Academic Publishers, 1995, pp. 293–336.
- [31] G. ZASLAVSKY, *The simplest case of a strange attractor*, Physics Letters, 69A (1978), pp. 145–147.